International Journal of Unconventional Science
Issue E2, pp. 23-40, 2017

received: 08.05.2018
accepted: 22.05.2018
http://www.unconv-science.org/e2/kernbach1


# Tests of the circular Poynting vector emitter in static E/H fields

Serge Kernbach*

***Abstract*—This paper describes tests of a compact Poynting vector generator utilizing the effect of a circular electromagnetic energy flow in static E/H fields. The generator is powered through USB port or 5V 'Power Bank' accumulator and represents a further development of the 'small Akimov's generator' on modern element base. The design of a circular CPV emitter allows scaling the emission effect and is compatible with passive generators 'Contur'. Control electronics can modulate output signals generating E/H fields for usage with different 'electronic modulators'. Performed tests with fluids and microbiological samples confirm electrochemical and biological effects of this generator. The device is developed as an EM actuator with environmental feedback loop for robotic systems, or as a tool for non-chemical treatment in infoceutical production and materials science, as well as for a long-range signal transmission in various applications.**

## I. Introduction

Electromagnetic generators of a weak emission based a Poynting vector in static E/H fields with circular or cylindrical emitters are popular in various designs. Such well-known devices as 'small Akimov's generator' (SAG), see Fig. 3, or 'large Akimov's generator' (LAG), see Fig. 15, are examples of these devices. There are several descriptions and assumptions about their underlying mechanisms [1], [2].

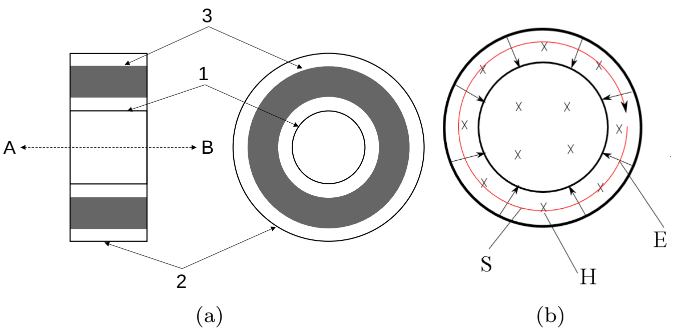


Fig. 1. **(a)** Structure of the SAG/LAG emitters: 1 – inner layer of a cylindrical capacitor, 2 – external layer of a cylindrical capacitor, 3 – ring magnet (or electromagnet). Emission is directed in the axial direction A-B; **(b)** Illustration of the circulating Poynting vector $S$ in static E/H fields, image from Wikipedia.

*Cybertronica Research, Research Center of Advanced Robotics and Environmental Science, Melunerstr. 40, 70569 Stuttgart, Germany, Contact author: serge.kernbach@cybertronica.de.com

The structure of these EM generators is based on the interaction of orthogonal magnetic **H** and electric- **E** fields, generating the Poynting vector. Some publications relate them to the so-called 'Tamm's emitters', in following we will denote all emitters of this type as the 'Poynting vector' emitters. The most common version includes a disk (ring) magnet and a cylindrical capacitor, see Fig.1(a). Instead of a permanent magnet, electromagnets are often used. A constant voltage is applied to the cylindrical capacitor, in SAG/LAG it varies about 100-200V. New designs of emitting elements have been appeared in the last years, they deviate from the SAG/LAG 'standard' attempting to create new versions of these devices. Examples are emitters of S.N.Tarakhtia, the modern development of a planar (PPV) emitter is undertaken by Vitaly Zamsha [3]. The active part of the generator, its emitter, is a planar construction with two Helmholtz coils and a flat capacitor, see Fig. 2. This design allows minimizing the parasitic capacitance between electrodes and the coil. However, tests also showed some disadvantages of PPV emitters.

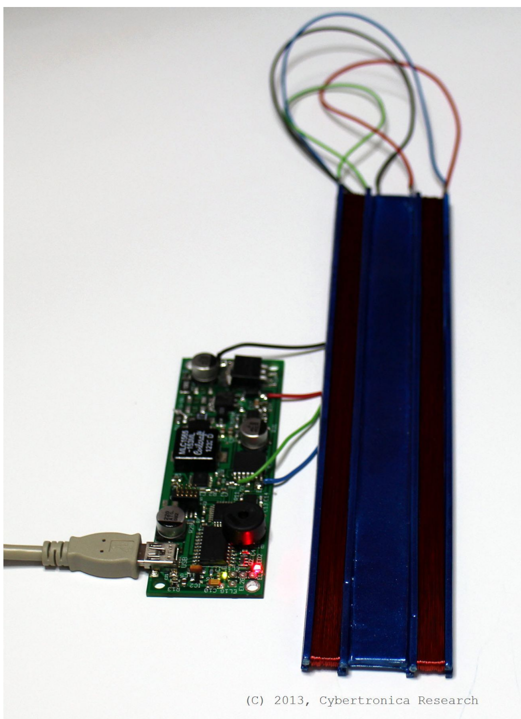


Fig. 2. Planar Poynting vector (PPV) emitter.

Fig. 3. One of the SAG constructions used in 80s and 90s.

The design of the SAG/LAG was confidential in the 90s (for example, these generators were sealed), at the moment there are several descriptions of their design [4], prepared, among others, by E.A.Akimov [1]. Organizations that collaborated with the MNTC 'VENT' (the organization that coordinates a Russian development in these areas in the 90s [5]) received this type of generator for experiments, mostly SAG, see Fig. 3, therefore the large number of experimental results was obtained for generators based on the Poynting vector. To some extent, the SAG represents one of the most successful devices of this kind with a great number of publications [6]. However, these proven and tested devices are almost impossible to acquire; this creates a certain need for their production.

As mentioned above, the working principle of 'Poynting vector emitter' consists in creating an orthogonal system of electric and magnetic fields. More formally, the Poynting vector $\mathbf{S}$ is the vector of energy flux density of the electromagnetic field, which can be defined by the vector product of two vectors:

$$\mathbf{S} = [\mathbf{E} \times \mathbf{H}], \tag{1}$$

where $\mathbf{E}$ and $\mathbf{H}$ are vectors of electric and magnetic field. Modern textbooks consider the case of Poynting vector in a cylindrical capacitor, which is located in the H-field created by a permanent magnet. Although only static electric and magnetic fields exist, the calculation of the Poynting vector gives a circular flow of electromagnetic energy clockwise, see Fig. 1(b). The flow of circulating energy underlies the popular idea of 'rotation' of the $\mathbf{S}$ vector, which is located in the axial plane in Fig. 1(a) (the circulating energy flow contains the angular momentum and creates the magnetic component of the Lorentz force arising when the capacitor is discharged). Such a 'rotation' component is missing in PPV. The circulating flow shown in Fig. 1(b) generated by the constant E/H fields led to the idea of a circular emitter in which the rotating Poynting vector will be generated 'outside' the emitter (not inside the cylindrical capacitor).

One of underlying ideas of this development is devoted to a non-chemical treatment of liquids and interactions with biological objects, similar to the magnetic vector potential [7], [8], [9]. Open research question, which could serve for explanation of arising effects, is the relationship between the circulating Poynting vector and the Aharonov-Bohm-type [10] or quantum-entanglement-type effects that manifest in macroscopic systems [11], [12]. This development also pursues the research of external feedback mechanisms to enhance long-distance interactions (for example, the 'Maslobrod effect' [13]). This issue has already been discussed in the literature: robots and mice/chicks [14], [15], thermostats with plants [16] and animals [17], mechanical oscillating systems [18], the Smirnov's emitter with feedback loops [19], etc. In this paper, the automation DA module [20] is used to create and operate the feedback elements.

This paper has the following structure: Sec. II describes the emitter and control electronics, Sec. III – the performed electrochemical and biological measurements, Sec. IV concludes this work.

## II. Development of the emitter and control electronics

The development of both the emitter and the control module was motivated by practical needs for a small device with applications for infoceutical production, e.g. for non-chemical treatments [21], [22], [23], the treatment in non-stationary EM fields [24], known also as the phase-transition-treatment (PTT) effect, as well as for different

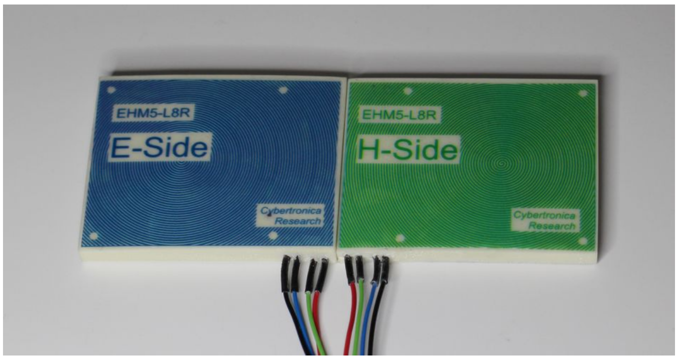


(a)

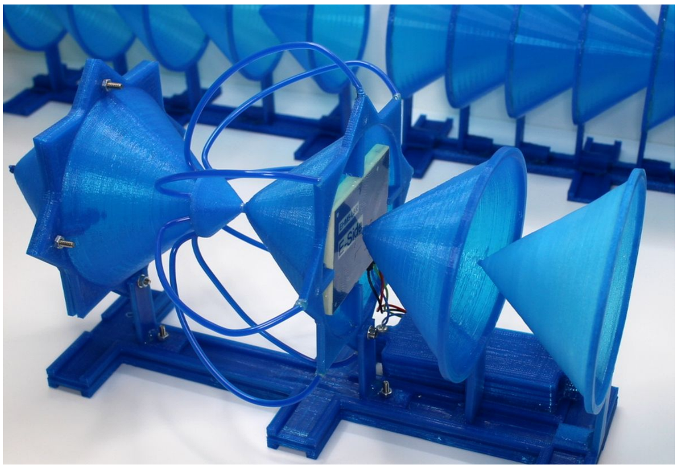

(b)

Fig. 4. **(a)** Multilayer circular Poynting vector (CPV) emitters in a monolithic body; **(b)** Generator based on the shape effect using a monolithic CPV emitter in 2013 [3].

distant phenomena [25]. Especial requirements represent the production technology, i.e. the device must not have parts requiring manual work, such as the wound coils. The generation of weak emission must be scalable at the level of the emitter – the emission strength of the basic device should be small, but allows scaling up or down the effect. From marketing reasons, it makes sense to develop not one single-block device, but a kit, where the user can configure the system, including other devices based on the shape effect. The control electronics must be powered by a USB port or the 'Power bank' accumulators with a 5V supply voltage, i.e. the device must be transportable.

Multilayer flat circular emitters has already been developed in research projects, where the multilayer Poynting vector emitters were produced in a monolithic casing, see Fig. 4. These emitters were also used in test generators based on the shape effect early 2013 [3]. However, at that time, the development was concentrated on the Bobrov's LED emitters [26] and the CPV concept was further followed. The advantage of a flat emitter is its high technological processability, since it can be mass-produced by the technology of printed circuit boards. However, the manufacturing complexity of a monolithic emitter required to reconsider its structure and to approach the open design of flat emitters shown in Fig. 5(a). It repeats the structure of the E/H fields in Fig. 1(b), but the cylindrical capacitor is replaced by the flat capacitor, and the permanent magnet is replaced by the double flat coil, i.e. the emission element represents a kind of 'circular dipole'. Obviously, the number of circular dipoles can be increased, see Fig. 5(e), which will scale up the effect.

A rotating Poynting vector **S** is generated in the outer part of the emitter. The emitter is mounted on a small cone, see Fig. 5(a) and can be used as a stand-alone device. However, sometimes it becomes necessary to 'transport' **S** to the vertex point of the cone for later use with the shape effect (in the SAG manner). Therefore, the emitter is mounted inside a large hollow cone, as shown in Fig. 5 (b,c). The outer cone also serves to protect the CPV emitter and to shield from EM fields. On a large cone, either a small cone for the PTT effect (with modulating substances embedded there) or a metal tip can be installed, see Fig. 5(c). These elements are known from the 'Contur' generator and are fully compatible with this popular structure based on the shape effect. Since modular structures are offered as a kit, it is even possible to create symmetrical emitters, see Fig. 5(d), known in LAG. The structure in a large cone shown in Fig. 5 (b,c) will be further denoted as the 'CPV emitter'.

The electronics module, which generates signals for the emitter, is shown in Fig. 6, its structure is shown in Fig. 7. It is a microprocessor system with two cascade circuits for increasing the voltage to 1200V, a current control circuit (up to 100 A in the pulse) and a modulation system for all voltages. A more detailed description of the EHM-C module is given in the appendix. The company has been manufacturing EHM-C modules for several years, there are several modifications with various enclosures and 5V,

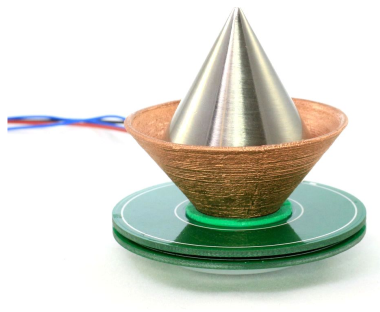

(a)

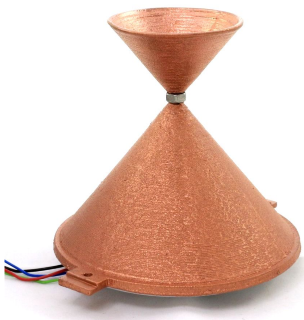

(b)

(c)

(d)

(e)

Fig. 5. **(a)** An open circular Poynting vector (CPV) emitter, mounted on a small cone; **(b,c)** Emitter from (a), mounted inside a hollow copper cone; **(d)** Symmetrical structural element used in LAG; **(e)** CPV emitter with an increased number of circular dipoles, mounted on the EHM-C module housing, the upper cone cap is removed.

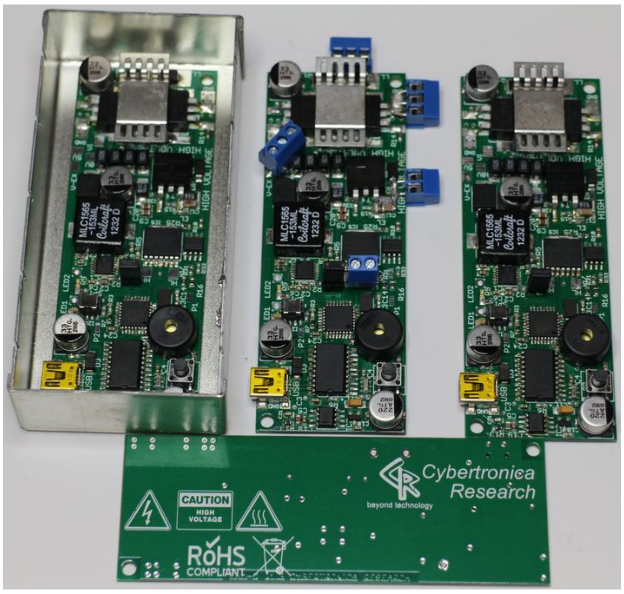


Fig. 6. The EHM-C control module.

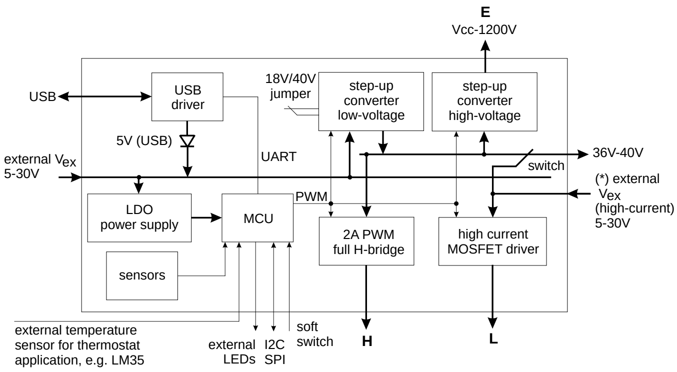


Fig. 7. The structure of the EHM-C control module.

12V and 24V power systems. The configuration of voltages and control approaches is set by the user through the client program on the PC. In experiments described below, about 1000V of DC voltage was supplied to the CPV capacitor and about 200 mA of current at 5 (or 12) volts to the CPV coils.

As already mentioned, the development pursues the principle of modularity, therefore all components are offered separately as several sets. For example, the CPV emitter can be mounted on the front part of a holder, and the EHM-C module at the rear, see Fig. 8(a). In a standard version, the CPV emitter is mounted on a solid aluminium housing with the EHM-C module that has an optional 5V power supply (from USB or 220V/110V) or 12V (from 220V/110V), see Fig. 8(a). The electronics allows reading the files generated by 'electronic modulators of PTT effect' and to modulate the E- or H-field components by the information from these files for a distant PTT effect with the selected electronic modulator.

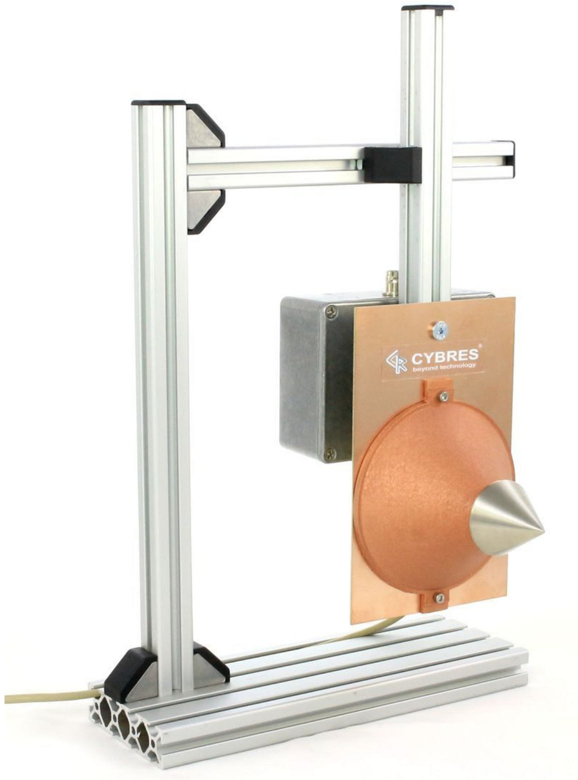


(a)


(b)

Fig. 8. Mounting the CPV emitter and the EHM-C control module on **(a)** the holder, **(b)** the housing.

## III. Performed tests with the generator

### A. *Control measurements*

The EIS devices with differential impedance spectroscopy are used as sensors in these measurements [27], [28], [29]. Measuring effects of EM generators of 'weak emissions' has some difficulties primarily due to temperature changes caused by the heating of coils and high-voltage electronics. Since the electrochemical sensors (outside the thermostat) react also to the temperature changes, it is necessary to 'untie' the temperature and non-temperature factors. In general, the relationship between temperature and electrochemical measurements (e.g. electrical conductivity) is nonlinear [30]. Since the degree of nonlinearity is relatively small in the range 0-30° C, a linear approximating equation is used [31]:

$$EC_t = EC_{25}[1 + a(t - 25)], \quad (2)$$

where $EC_t$ is the electrical conductivity at temperature $t$, $EC_{25}$ is the electrical conductivity at 25°C, and $a$ is the temperature compensation coefficient. In the work [32] various values of $a$ in the range of 0.0191-0.025 are considered. For small temperature changes e.g. $\Delta t < 1$°C, we can assume that $EC_t$ follows temperature with a certain coefficient. Large nonlinear variations of $EC_t$ are introduced by non-temperature factors.

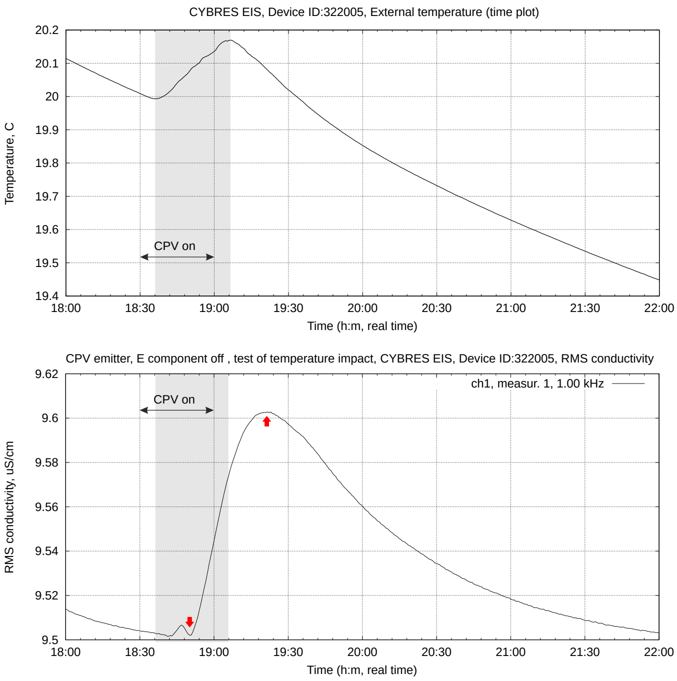


Fig. 9. EIS measurement of temperature dependence (2). The E-field is disabled, the Poynting vector is not generated, the temperature change occurs only due to heating of the coils. Time interval between inflection points of temperature and EIS curves (when turning the coil on and off) is about 7 minutes.

To confirm this statement, the EIS measurement was performed when the high-voltage part was switched off. The 5V voltage applied to the coils caused heating of the CPV emitter without generating the Poynting vector. For these tests, the electronic EHM-C module was disconnected from the emitter and moved out of the closed experimental chamber, so the temperature changes occurred only due to the heating of the emitter. To reduce heat production, the current was reduced to 2/3 of the maximum value, in addition the modulation with 50% meander applied, i.. all tests passed at 1/3 of maximal power. The temperature sensor and the measuring container with

(a)

(b)

Fig. 10. Spectrograms **(a)** of alternating electric and **(b)** alternating magnetic fields at the distance 10mm from the grounded copper cone, the CPV emitter with the EHM-C generator is running. The measurement was carried out by the Spectran 5010 low-frequency spectrometer.

water were mounted on the top of the large cone, see Fig. 5(b). The result of this EIS measurement is shown in Fig. 9. The EIS dynamics without the generating the Poynting vector, follows closely the temperature trend, as described by the equation (2). The time interval between inflection points of temperature and EIS curves is similar when the coil is turned on and off.

The second issue required to consider at such measurements is the electromagnetic shielding of both the control electronics modules and the emitters. To do this, all components of the generator are in metal housings, the copper cone of CPV emitter was grounded to a common ground wire. EM emission was measured with the Spectran 5010 device in the range from 100Hz to 1MHz, the spectrograms are shown in Fig. 10, the device was located at a distance of 10 mm. from the cone. The intensity of alternating electric

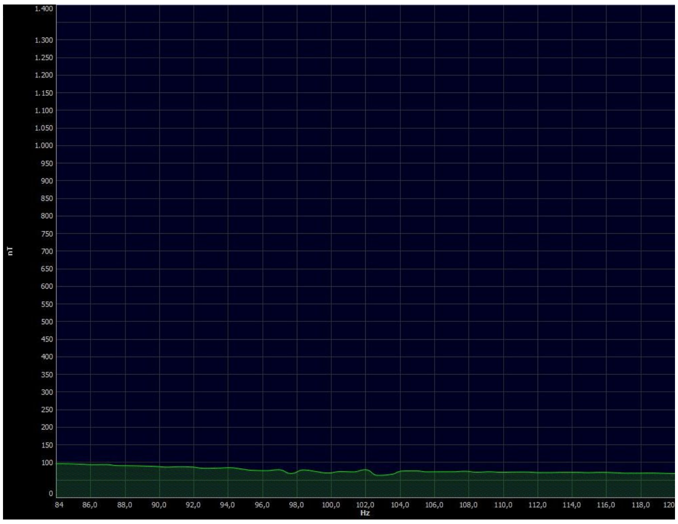

Fig. 11. Measurement of the alternating magnetic field when the H-field of the CPV emitter is set to the frequency of 100 Hz.

field does not exceed 30V/m in the low-frequency part and not more than 4V/m at frequencies up to 1MHz. The intensity of alternating magnetic field does not exceed 100 nT in the low-frequency region and 10 nT at frequencies up to 1 MHz. These values are extremely low for rooms and do not change when the generator is turned on or off. For additional tests, the magnetic part of the CPV emitter was excited at the frequency of 100Hz and the H-field was measured in the range 84-120 Hz, see Fig. 11. This modulating frequency is not detected by Spectran 5010 near the emitter. Thus, these measurements allow us to conclude that the shielding of both the CPV emitter and the electronic module is sufficient.

### *B. Measuring the emission effects*

For measuring the effects of generated weak emission, one EIS sensor was mounted on the top of the cone, the second one was installed on the side (near the cone so that sensor touches it). This arrangement allows estimating the contributions of axial and radial components of the emission. The temperature sensor was installed at the top and at the side locations. Figure 12(a) shows the case when the EIS and temperature sensors are mounted in the top position, it corresponds to the experiment shown in Fig. 9, when the E-field is turned on and the Poynting vector is generated.

The generator was operated for 20 minutes, the temperature change was about 0.15° , which is similar to the previous temperature test. However, the inflection points are positioned in this case differently, the starting point is closer to the temperature inflection, and the final point is shifted by 45 minutes after the temperature inflection (the 7 min. time interval between both points in the temperature test was almost equal to each other). These data point to other factors, beside temperature, that influence the EIS dynamics. We note once again that the

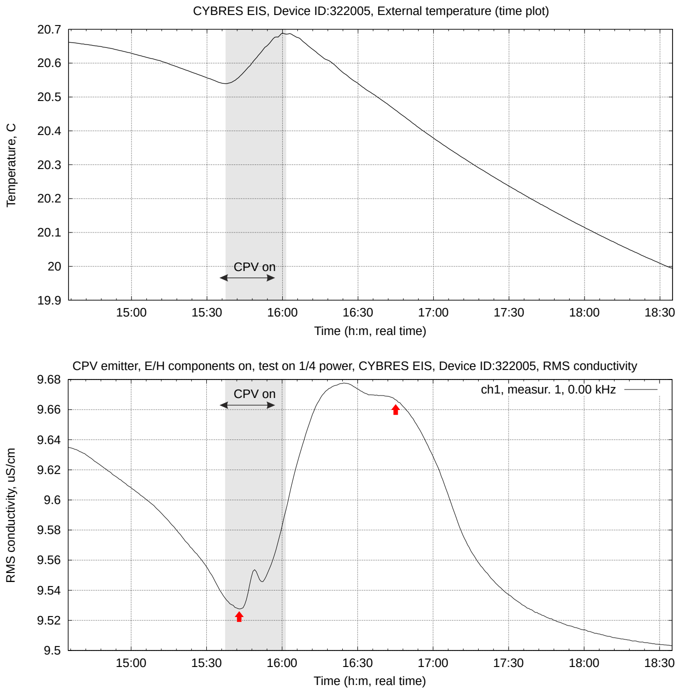


(a)

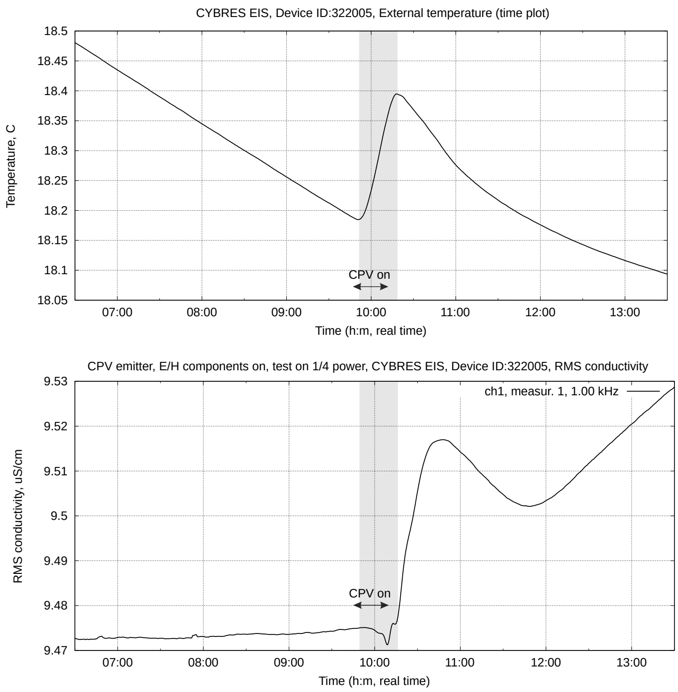


(b)

Fig. 12. **(a)** EIS measurement at the top of the cone, E/H fields are on, the Poynting vector is generated. Time interval between the first inflection points of temperature and EIS curves is about 3 minutes, the second inflection points – about 45 minutes; **(b)** EIS measurement of the activated fluid from the previous experiment performed on the next day. The 'paradoxical phase' is observed, which violates the temperature dependence expressed by the equation (2).

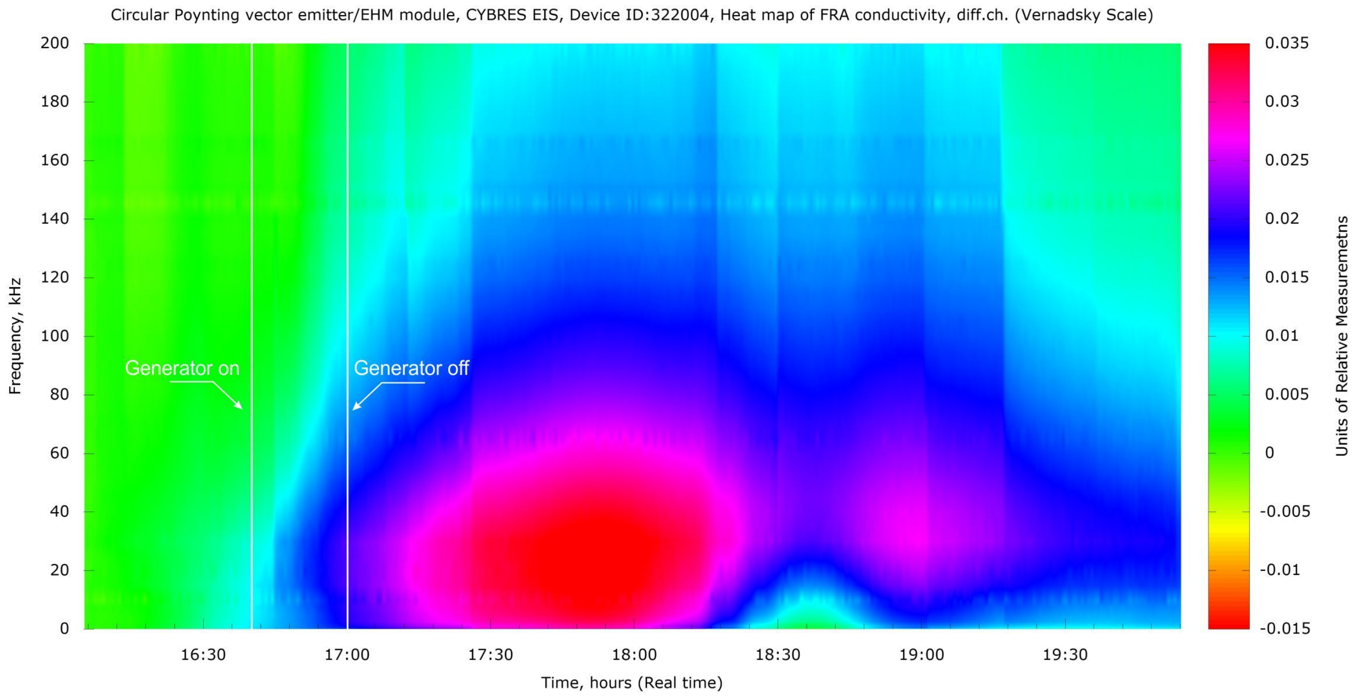


Fig. 13. EIS dynamics, the turn-on time of the generator is shown by lines, the appearance of (quantum) proton tunnelling effect in the form of jumps in the graph is observed, the operating time of the generator is 30 minutes, the post-EIS dynamics (disappearance of changes) is about 180 minutes.


Fig. 14. CPV emitter without a closing cone, mounted on a plastic holder.

conditions of both experiments are identical, the EM factor is eliminated by EM shielding, all experiments are carried out without light (full darkness). We also observe a higher intensity of the reaction. The EIS change in Fig. 9 was about 0.1 $\mu S/cm$, the EIS change in Fig. 12(a) is 0.16 $\mu S/cm$, i.e. almost 60% more intensive.

It is known that the exposed by emission fluids behave electrochemically different than non-exposed fluids. For example, the performed tests [33] demonstrated the appearance of a 'paradoxical phase' that violates one of the fundamental electrochemical dependencies – the temperature dependency expressed by the equation (2). For tests of this phenomenon, the water activated in the previous experiment was left for one night in measurement chamber, and the second EIS measurement was performed on the next day. The result of this second measurement is shown in Fig. 12(b), where the 'paradoxical phase' is clearly visible – in response to decreasing temperature, the amplitude of the EIS dynamics increases.

For further tests of the axial direction, the CPV emitter was taken out of a cone and mounted on the holder, see Fig. 14. The emitter was placed on a plastic part to decouple it from the grounded housing of the control module. The idea is that grounding of the cone can affect its efficiency, i.e. part of the 'weak emission' flows down to the ground. To prevent EM impact, a grounded sheet 0.3 mm of steel with a size of 300x200 mm is installed between EIS sensors and the CPV emitter. Despite this shielding is not not full (i.e. it does not create a Faraday cage), the goal of this test was to demonstrate changes that can last for hours after the generator was turned off. Such long-term post-experimental changes are uncharacteristic for EM emissions.

Results of these EIS measurements are shown in Fig. 13. The response of EIS sensors starts with a delay of about 2.5 minutes (the distance between the radiator and the sensors is 20 cm), and there is no change of temperature trend on the sensor side. When the generator is turned off, the effect slowly disappears: with a 30-minute operation of the generator, the post-experimental EIS dynamics (disappearance of changes) takes about 180 minutes. The spikes in the graph after exposure indicate the effect of proton tunneling in water, responsible for the anomalous conductivity. This effect was also observed in other tests with non-local EM generators. Thus, both the duration and the characteristics of the EIS changes after turning off the generator are uncharacteristic for EM emissions, and indicate other causes of their occurrence.

### C. *Tests of axial and radial effects*

As mentioned above, the state-of-the-art effects published in relation to the Poynting vector in static E/H fields with circular emitters (see e.g. [34]) were taken into account in the design of CPV emitter. As known, such weak emissions exhibit some optical and electrical properties, in particular they are 'transported' along metal conductors, and 'concentrated' by conic geometrical shapes. These effects were also considered in the design of LAG, which possesses different conic elements connected by metal wires, see Fig. 15. Here we observe a further development of ideas from SAG, see Fig. 3, in particular all emitting elements are not grounded (only the main housing is grounded). LAG also provides an interesting example of combining different types of weak emission by passive structural elements.

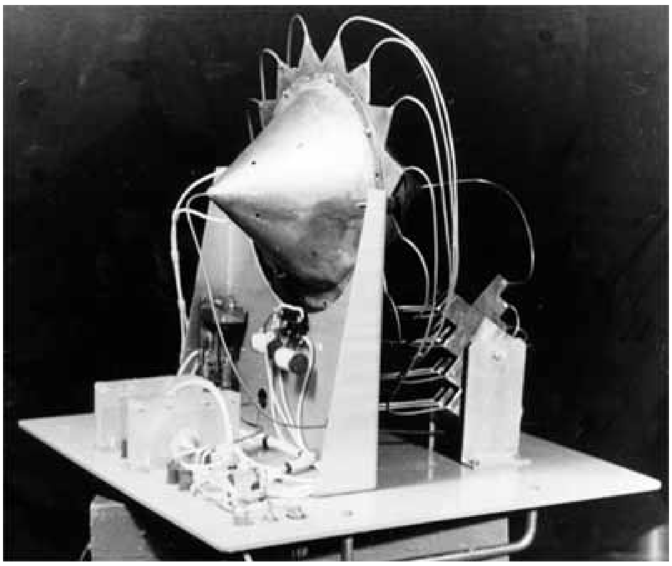

Fig. 15. Structure of LAG, usage of different geometric elements and metal wires, image from alt-sci.ru.

Returning to the CPV emitter, it is expected that the metallic cones should have two effects: firstly, the emission will be 'collected and transported' to the top, and secondly, the grounding will reduce the effect due to 'leakage' of 'weak emission' to the ground. The possibility of such a leakage is also indicated by other experiments, e.g. by the well-known Hieronymus's experiment with plants [35].

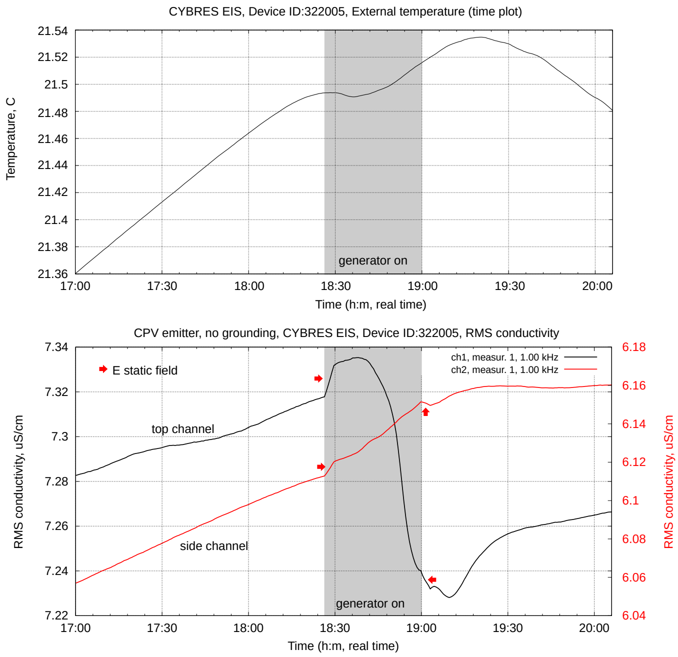


Fig. 16. Tests for axial and radial effects, channel 1 is installed on the top of the cone, channel 2 on the base, the containers touch the metal cone, the grounding of copper cone is removed.

To test this hypothesis, the previous setup was used – one EIS container at the top of the cone, the second on the side on the base, both plastic containers with water touch the metal cone. The cone grounding is removed, the temperature sensor is mounted on the side container. The result of the EIS measurement is shown in Fig. 16. An obvious effect is the potential jumps when the generator is turned on and off, which is explained by the appearance of a static E-field. Based on the example of channel 2, we can conclude it affects the EIS dynamics, but its contribution is small even in comparison with the temperature effect. The channel 2 located in the radial direction follows a temperature trend, whose variation is smaller since the temperature sensor does not touch the metal cone. There is a faster reaction of the EIS sensors compared to previous experiments with grounded cones (however, here the question arises of the contribution of the static E-field). Comparing the axial and radial arrangements, we can see that changes in the axial arrangement (channel 1) at the top position are much more intense, which may point to the 'transporting' effect of the emission.

Similar data were obtained in other experiments, for example Fig. 17 shows both channels of the previous experiment performed with another set of electrodes. The EIS channel at the top position of the cone has a larger amplitude and a faster response, which indicates a predominance of the axial direction in the generation of weak emissions.

### D. *Measuring effects of liquids exposure*

The well-known application of SAG/LAG (and similar generators whose development was inspired by SAG/LAG)

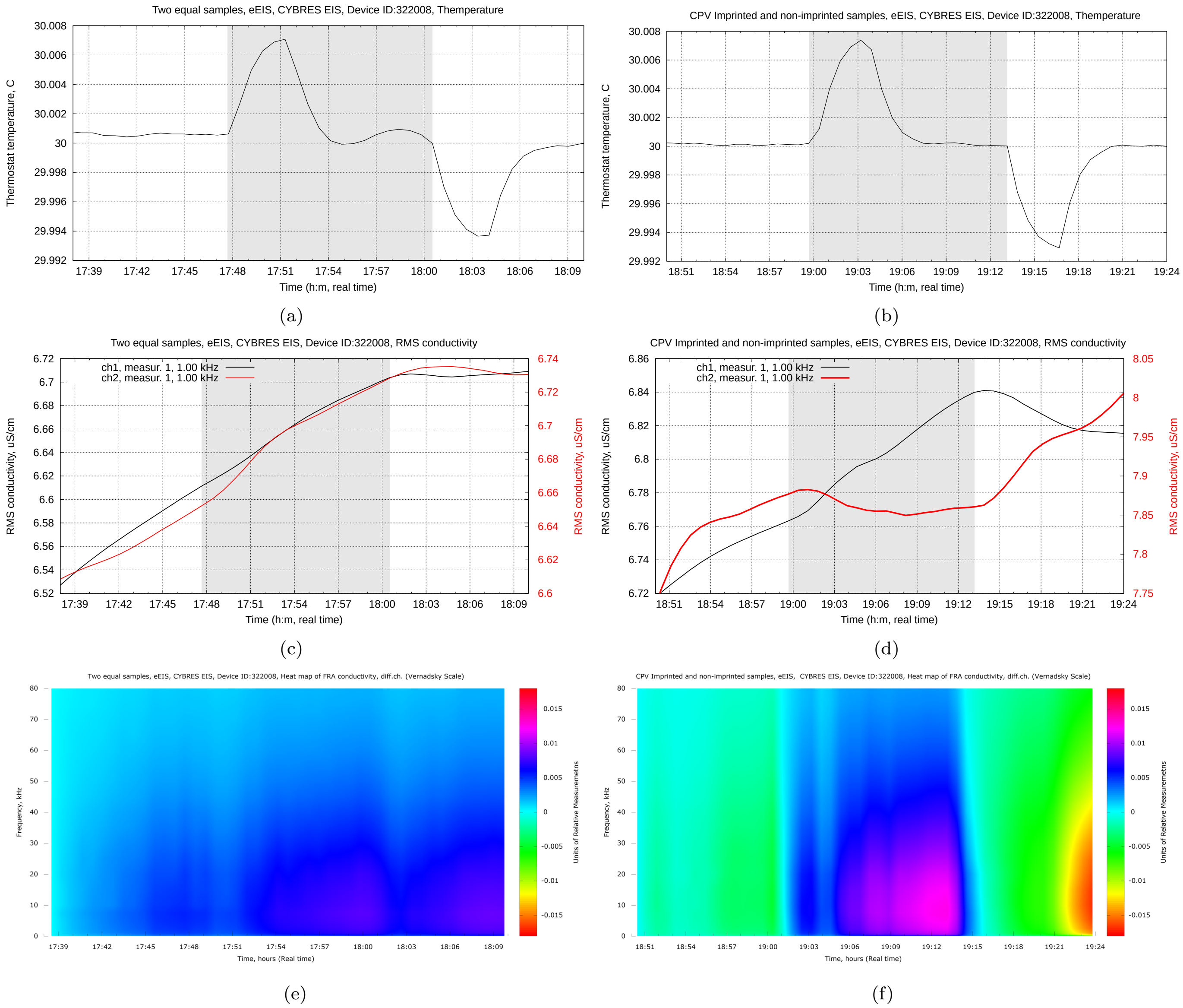


Fig. 18. Express analysis of two pairs of fluids: **(a,c,e)** analysis of two identical not-exposed-by-emission fluids in the control pair; **(b,d,f)** analysis of two liquids in the experimental pair, one of which was exposed for 30 minutes at the top position of the CPV emitter. Degassing of fluids (repeated removal of electrodes from containers) was not performed for both attempts.

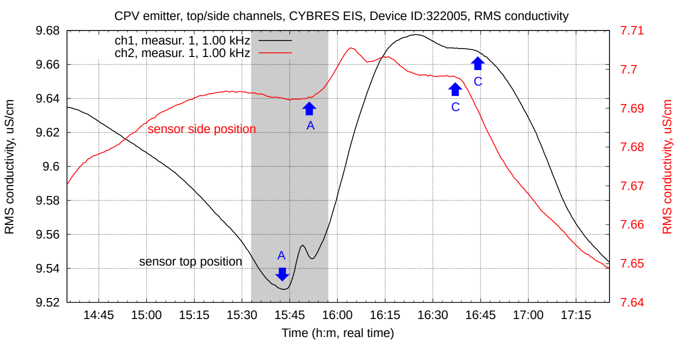


Fig. 17. Tests for axial and radial effects, comparison of the EIS channels mounted on the top of the cone and at the base, see the previous experiment, shown in Fig. 12(a).

was the exposure of liquid and solid substances with and without PTT effect, after that these materials demonstrated different physical and chemical properties. Figure 19 demonstrates the SAG-based setup, used for exposure of solid materials in experiments around 2000 in South Korea. It needs also to mention multiple successful experimental results of using such EM generators in metallurgy with PTT [24].

The works of V.A.Sokolova [36] were especially intensive in this respect, we already repeated some experiments of this group [29]. In these experiments, two identical samples were prepared and compared by the impedance spectroscopy, then one of them was irradiated by a generator without PTT, and then these two samples were compared again. Figure 18 shows the results of a similar experiment, carried out by the modern method of EIS

Fig. 19. Experimental setup based on SAG and used for exposure of solid materials, 2000, Seoul, South Korea, photo courtesy of A.Y.Smirnov.

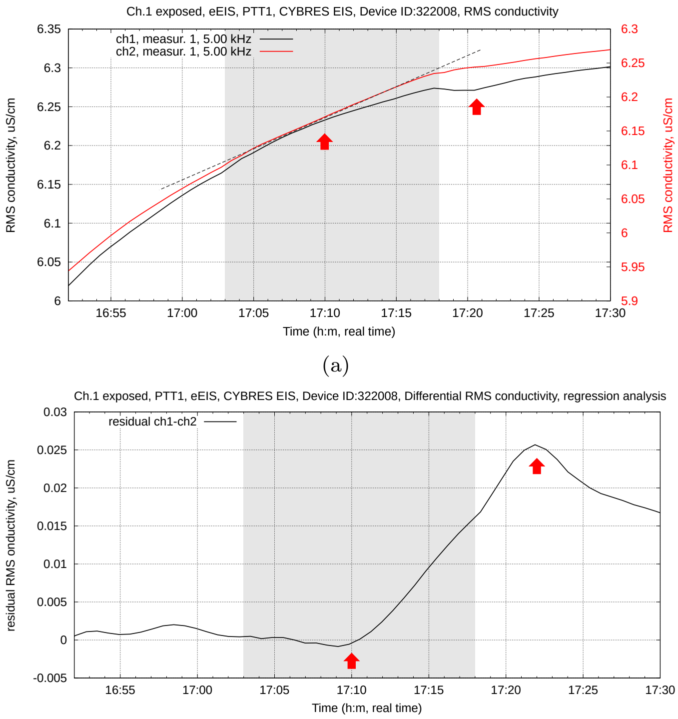


(a)

(b)

Fig. 20. Exposure of liquids, PTT1, the sample N5, the channel 1 is the exposed (experimental) channel, the channel 2 is the control channel; **(a)** two channels representation; **(b)** the regression analysis of differential channel, see description in text. Degassing of fluids was performed.

express analysis. Four samples (two pairs) of 10 ml of distilled water are prepared. One pair represents a control pair for the differential measurement, one liquid in the second pair was irradiated for 30 minutes at the top position of the CPV emitter. That pair represents an experimental pair for the differential measurement. Both pairs were prepared and analyzed in a similar way in the thermostat, the same time was given for temperature equalization, moreover, all samples were analyzed for a short time one after the other – first the control pair, then the experimental pair. As shown by Fig. 18(c), the behavior of the EIS curves in the control pair is very similar, their differential spectra in Fig. 18(e) are rather homogeneous. The behaviour of the experimental pair in Fig. 18(d) differs substantially from each other, their differential spectra in Fig. 18(f) shows a characteristic pattern of differences. Thus, we observe a similar effect with the results obtained by the Sokolova's group – an irradiation for a short time substantially changes the electrochemical dynamics of the exposed liquid.

For further tests with exposed liquids by PTT effect, we used the generator shown in Fig. 8(b) powered by 12V (from 110V/220V AC-DC converter) with one circular dipole element. The maximal current through coils was increased up to 0.4A with about 1000V on the capacitor. The regression analysis was employed for detecting differences between exposed and unexposed fluids, other parameters are similar to the previous tests. For the PTT with $C_{12}H_{22}O_{11}$ (denoted as PTT1), 12g. of the substance was placed in the small upper cone. The EIS container was placed on the top without touching the walls of copper cone. The experimental parameters are similar to the previous attempts: exposition time 20 minutes, all samples are exposed one after another within a short time interval. In the first day we performed 5 attempts, the exposure-measuring-cycle of one sample took about 1 hour. The first noted issue is the variation of intensity from 1st to 5th sample – usually the first exposed sample demonstrated the strongest results, like shown in Fig. 18. Secondly, exchanging control and experimental channels of the EIS spectrometer in following after each other measurements led to unstable EIS dynamics of both channels. The best conditions are long resting time between expositions, using the same control/experiment channels within one experimental series and different plastic containers in each attempt. In Fig. 20 we demonstrate the eEIS measurement of the last 5th sample, it is well visible that the exposed channel 1 behaves differently that the unexposed channel 2. In fact all inflection points of the differential curve obtained by regression analysis are caused by the exposed channel 1.

To test the results on technological or measurement artefacts, we repeated these attempts on the next day, but changed the impacted channel – now the channel 2 was the exposed channel, and the channel 1 is the control channel. The regression analysis of differential channel is shown in Fig. 21. We observe here the inverse type of dynamics of the Fig. 20(b) pointing to absence of technological artefacts in the measurements. There are also some variations of intensity and timing of inflection points that can be attributed to slightly different conditions of these repeated experiments.

Several control experiments with unexposed fluids and degassing procedure was performed between the PTT1 and

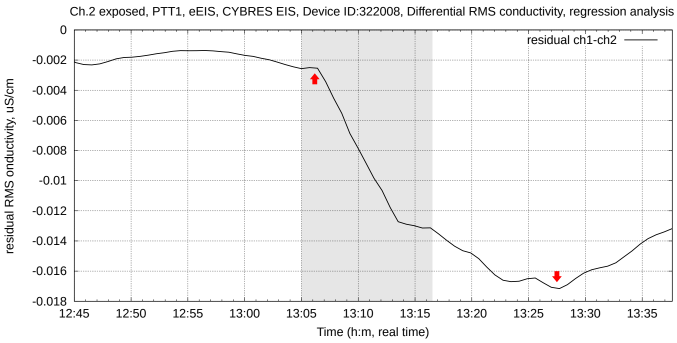


Fig. 21. Example of repeated attempts with changed channels, PTT1: the channel 2 is the exposed channel, the channel 1 is the control channel. Shown is the regression analysis of differential channel, see Fig. 20(b). The exposure time is doubled, the degassing of fluids was performed.

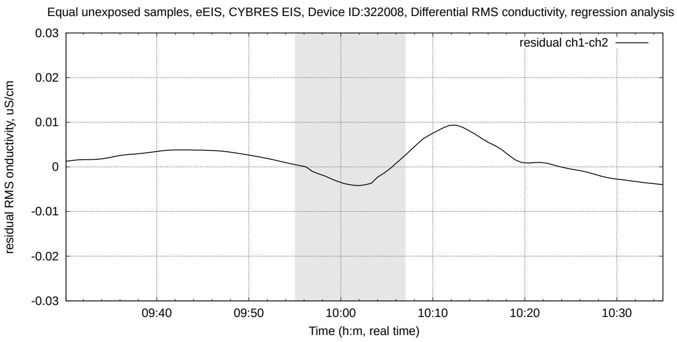


Fig. 22. Control attempt with unexposed fluids, the degassing of fluids was performed.

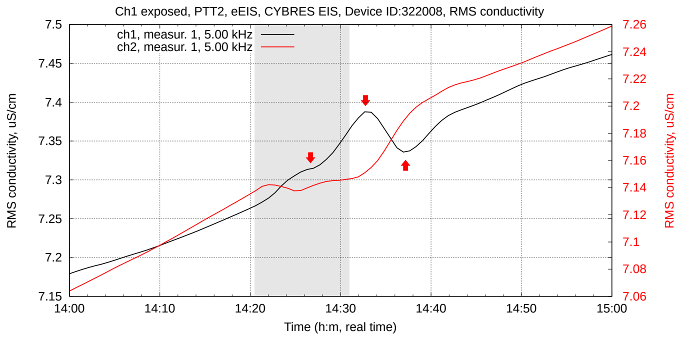


(a)

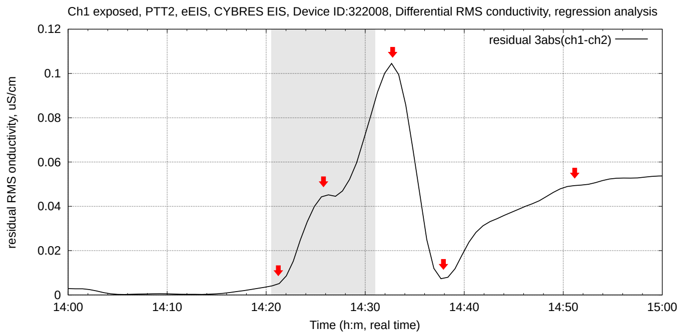


(b)

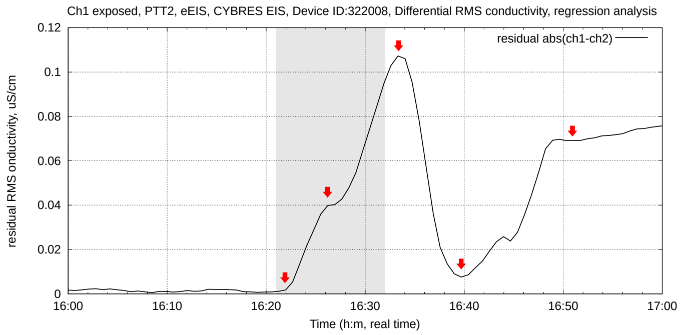


(c)

Fig. 23. Exposure of liquids, PTT2, the channel 1 is the exposed (experimental) channel, the channel 2 is the control channel, the degassing of fluids was performed. **(a)** Two channels representation, characteristic changes are in the exposed channel 1; **(c,d)** Two measurements with linear transformation performed within 120 minutes.

the next attempts with PTT2, one of them is shown in Fig. 22. In fact we observe a similar behaviour as shown in Fig. 18, however with smaller amplitude of variation. The final series of experiments were the attempts with $NaCl$ (denoted as PTT2), all parameters are similar to the PTT1 experiments. One experimental result is shown in Fig. 23, we observe the residual EIS dynamics that differs from PTT1 and control measurements that can be accounted to PTT2 effect (among other factors) in the exposed channel 1. We performed two measurements within 2 hours, which demonstrated a similar dynamics (with linear transformation required due to linear shift of differential curve) – this points to a reproducibility of results. 3D Spectrograms of data from Fig. 23 are shown in Fig. 24, which demonstrate interesting symmetrical activation patterns.

Experiments with the PTT effect continue further, for example, for accumulating statistically significant results and exploring additional effects that impact the exposure. However considering a limited focus of this paper devoted to tests of the CPV emitters, these results will be presented in a separate paper.

### *E. Measuring biological effects*

For testing biological effects, the CYBRES Biosensor based on the fermentation activity of yeast *Saccharomyces cerevisiae* was used. The experimental samples of water with sugar are exposed on the generator for 60 minutes, see Fig. 25(a). After this, the experimental and control samples were rested in the water bath for 10 min to equalize the temperature and then the yeast solution were added to the containers.

For analyzing the results, we used the phase characteristics – specific stages of fermentation start earlier (or later) depending on stimulating (or inhibiting) effect of exposure. For identification of a phase the differential RMS impedance is utilized, see Fig. 25(b), different stages of fermentation are characterized by an essential change (e.g. different slope) of EIS dynamics, see for more detail [37]. As required by the double differential measurement approach, we performed two measurements: first, the channel

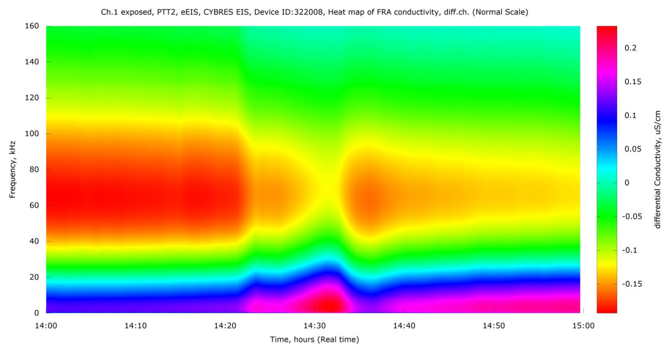


(a)

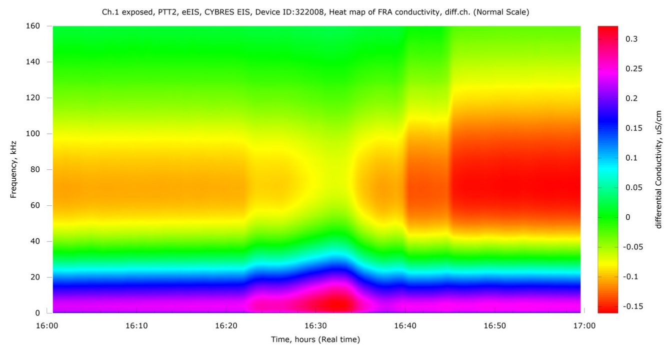


(b)

Fig. 24. 3D Spectrograms of two attempts from Fig. 23.


(a)

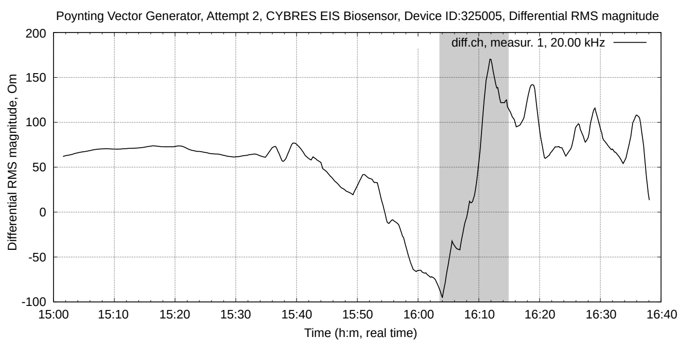


(b)

Fig. 25. **(a)** Exposing experimental samples of water with sugar (for biological tests) on the generator; **(b)** Identification of different phases of fermentation based on the dynamics of differential RMS impedance.

1 was the experimental channel, in the second attempt the channel 2 was experimental one. This approach enables identification of measurement artefacts and errors.

Figures 26(a) and 26(b) show the EIS dynamics of both control and experimental channels for these two attempts, the identified fermentation stages are shown by a grey bar. The resulting phase difference between control and experimental channels for both attempts are shown in Fig. 26(c). We observe more earlier start of fermentation in the exposed channel in both attempts, this points to a stimulating effect on activities of microorganisms by the generator.

### F. *Using feedback mechanisms*

Effects of nonlocal feedback loops in unconventional experiments has been studied since 80s of XX century. For example, [14], [15], [16], [17] discuss the interaction of a random number generator with plants and animals, where the nonlocal feedback is used to optimize the level and dynamics of illumination. The works [38], [39] demonstrate an appearance of 'untypical' oscillations in measured data for devices operating a long time in the same room. Malfunctions of devices, even the failure of temperature sensors and electronic components, are reported in cases of emotional events. Several experiments show a reaction of exposed fluid in closed containers on external UV light, while the control channels did not demonstrate any reaction in similar conditions [40]. Involving of human operators in feedback loops is discussed in some experimental setups [41]. These and other experiments indicate the possibility of spontaneous and targeted nonlocal loops between actuators and measured objects. It is assumed that introducing a nonlocal positive feedback can lead to 'self-excitation' of a remote object.

The automation DA module was used for tests with feedback elements [20]. This module is included in the EIS device and allows analyzing measurement data in real time – with so-called virtual detectors – and automatically operate various actuators in real world. These experiments were performed with two water containers as 'entangled objects', see Fig. 28. EIS measurements used external electrodes (outside of the thermostat) with temperature

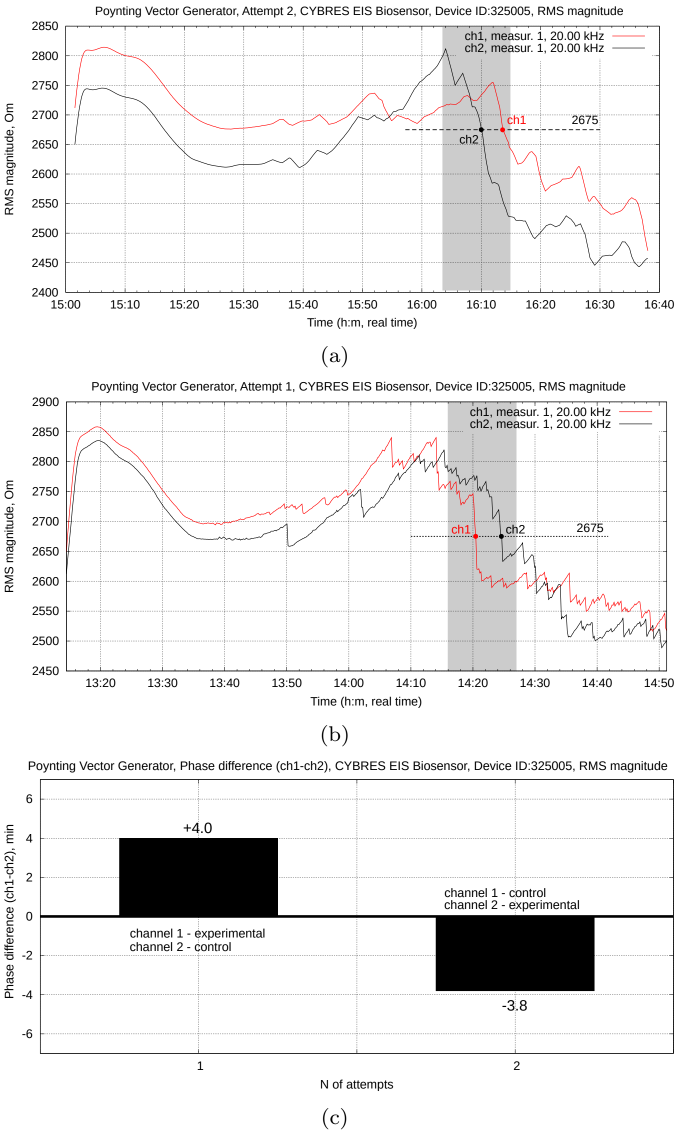


Fig. 26. Biological tests with CYBRES Biosensor based on the fermentation activity of yeast *Saccharomyces cerevisiae*. Two double differential attempts with inverse channels (the attempt 1: the channel 1 is the experimental channel; the attempt 2: the channel 2 is the experimental channel) are shown. **(a,b)** EIS dynamics of control and experimental channels for attempts 1 and 2, the identified fermentation stages are shown by a grey bar; **(c)** the resulting phase difference between control and experimental channels for both attempt, the exposed channel in both attempts demonstrate a stimulating effect on activities of microorganisms.

sensor inside fluids, i.e. the temperature of liquids was constantly measured.

In the first experiment, low-power red and green lasers (650nm, 532nm, power <1mV) were used as actuators for the channel 1, the condition $x > data[i] > y$ for RMS impedance represented a detector (the detector D21 from the DA module) for the channel 1. Parameters were adjusted so that a signal between $x$ and $y$ turned the lasers on, otherwise the lasers were turned off. Thus, a positive feedback loop was created, which should lead to oscillations in the channel 1.

Indeed, the appeared oscillations had the amplitude of 5-10 times greater than the noise during control measurements, see Fig. 27(a). An interesting effect is the uncontrolled (uncharacteristic) rise of impedance with the amplitude 50-100 times greater than the noise, see Fig. 27(b). After this rise, the sensor was no longer oscillating and apparently did not react to other weak signals (we already reported a loss of sensor's sensitivity after strong nonlocal effects [42]). The temperature dynamics in Fig. 27(c) does not explain such a dynamics of RMS impedance. It is assumed that the above-mentioned 'self-excitation' occurred, which however differs from a 'classical scenario' of loosing stability through an increase of the oscillation amplitude.

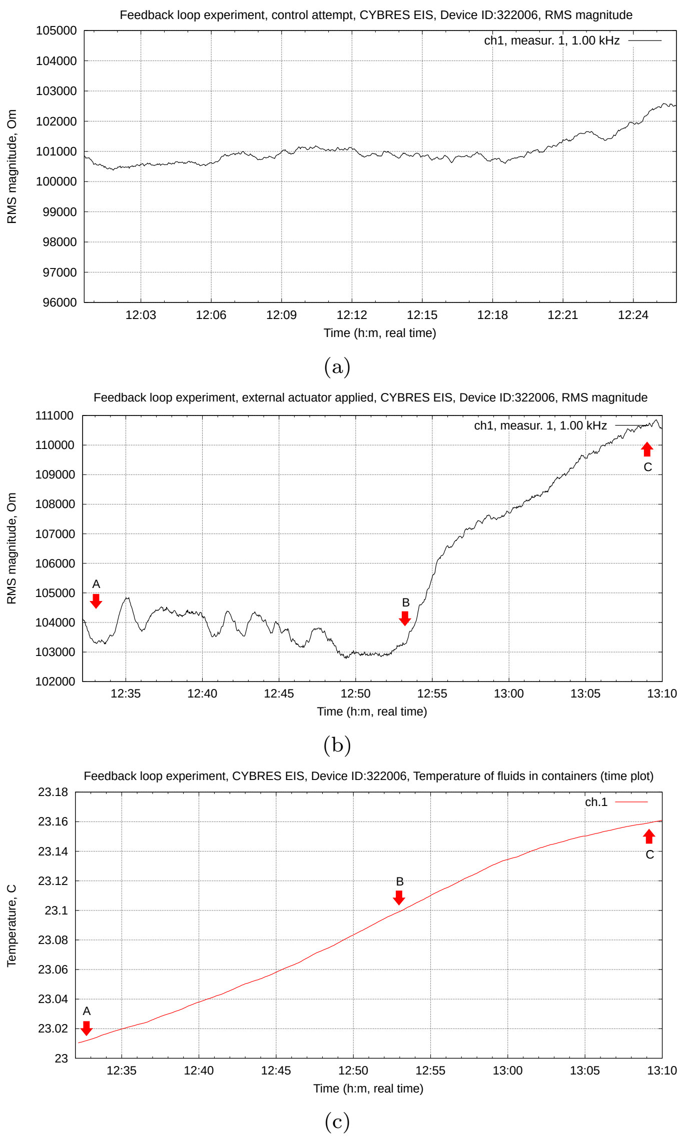


Fig. 27. Experiment with positive feedback in the local case. **(a)** Control measurement – unperturbed dynamics of channel 1; **(b)** The disturbed dynamics of channel 1 with the feedback loop, the area A-B shows an appearance of oscillations, the area B-C – a rise of impedance; **(c)** The liquid temperature during the experiment, changes of the RMS impedance cannot be explained by the temperature dynamics.

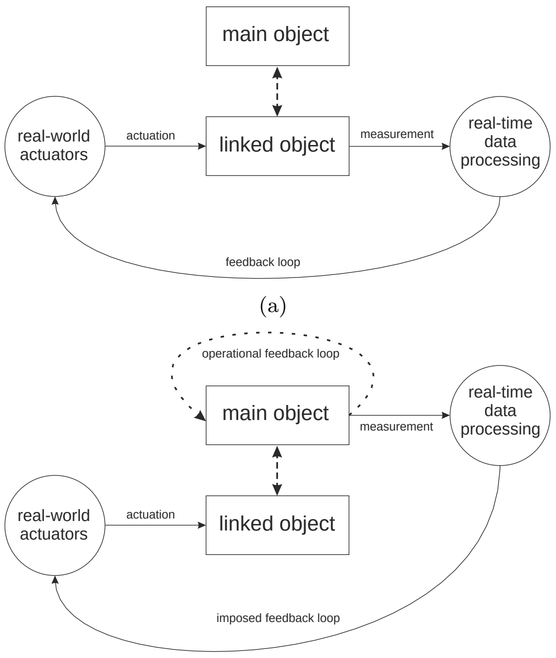


(b)

Fig. 28. Two types of possible feedback loops in 'macro-entangled' systems of 'main' and 'linked' objects. **(a)** The 'main object' does not have an intrinsic dynamics, the forced behavior is imposed on the 'linked object' through the feedback loop; **(b)** The 'main object' has a complex intrinsic dynamics, the measuring components are attached to the 'main object', feedback components – to the 'linked' object.

For the nonlocal case, it is necessary first to consider two types of possible feedbacks in 'macro-entangled' systems. In the first case, the feedback loop with forced behavior is established in the 'entangled' (linked) object, see Fig. 28(a). This scheme provides an acceptable control mode for the 'main object' if it does not have an intrinsic dynamics. In the second case, the 'main object' is assumed to have a complex intrinsic dynamics, therefore the measuring components are attached to the 'main object', see Fig. 28(b), and the feedback components – to the 'linked object'. The obvious difficulty of this method is the inaccessibility of the 'main object' for direct measurements and treatments; in practical situations it is necessary to use the nonlocal method from the first scheme. Thus, both approaches have advantages and disadvantages.

We used the differential EIS device for tests with 'macro-entangled' objects. An interesting correlations in dynamics of EIS channels have been observed in some specific cases, e.g. if the water for two EIS containers originates from one source processed by weak emission (see discussion later in text). Thus, the first EIS channel – as the 'linked object' from Fig. 28 – was used for exposure by the CPV emitter and laser, the second EIS channel – as the 'main object' from Fig. 28 – was placed about 0.5 meters away in a closed light-proof box. Both containers are covered by light and temperature isolation material, see Fig. 29.

To activate the CPV emitter and lasers, independent signal detectors were used, i.e. they operated in an uncoordinated manner and their activation patterns did not repeat throughout the experiment. Some influences, for example strong electrostatic fields, impact the entire measuring system, but others, such as a laser exposure on the first channel, do not affect the second channel (if both channels are optically separated from each other). The initial hypothesis of this experiment was that the created positive feedback through the electrostatic field (the cone of the generator is not grounded), effects of the Poynting vector and laser radiation in the channel 1 will be reflected to some extent in the channel 2, however, the electrochemical dynamics of the first channel will be unique and different from the dynamics of the channel 2. The experiment should indicate whether the 'self-excitation' from the first (linked) channel can be transmitted to the second (main) channel through a nonlocal 'entanglement' between containers with water.

Fig. 29. Light and temperature isolation of both channels (13mm PE).

The temperature dynamics of both channels in this experiment is shown in Fig. 30(a), the EIS dynamics – in Fig. 30(b). The operation of CPV emitter and lasers occurred in the 'on-off' modulation mode, the corresponding electrostatic modulation of the channel 1 is clearly visible. The channel 1 demonstrates various dynamics, such as oscillations, jumps, step-wise decays etc., which is explained by the internal electrochemical dynamics of water and three uncoordinated influences. Considering the dynamics of the channel 2, we see some differences, firstly in the amplitude (almost 10 times less). However, in general, the dynamics of channels 1 and 2 is correlated. Especially characteristic are the 'steps' marked with blue arrows in Fig. 30(b). Since the electrostatic impact is equal at any time, the appearance of 'steps' reflects only the EIS dynamics of fluids and it must be unique for each container. Even if 0.5 meter does not represent a significant obstacle to a radial emission from the generator, we still expect differences in the dynamics of both channels. The appearance of correlations indicates that either there is an instrumental parasitic connection between channels (its absence is easy to verify, see Figs. 31 and 32(a)), or there is an additional synchronization of dynamics, in the

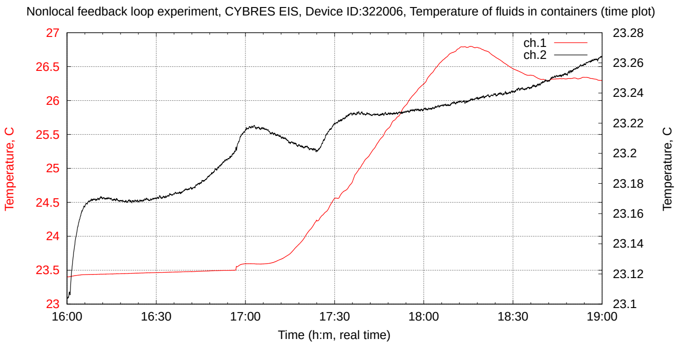


(a)

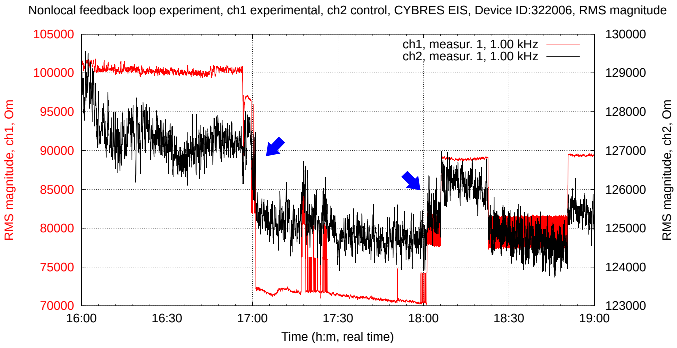


(b)

Fig. 30. Experiment with positive feedback in the nonlocal case between containers with water filled from one source and treated by weak emissions. **(a)** The temperature dynamics of both channels, variation of temperature in the channel 1 about 4°, in the control channel about 0.18°; **(b)** EIS dynamics of both channels without averaging filter, the excitation voltage is set to the minimum scale of 0.01V-0.1V, the modulation by the CPV emitter in the channel 1 is visible.

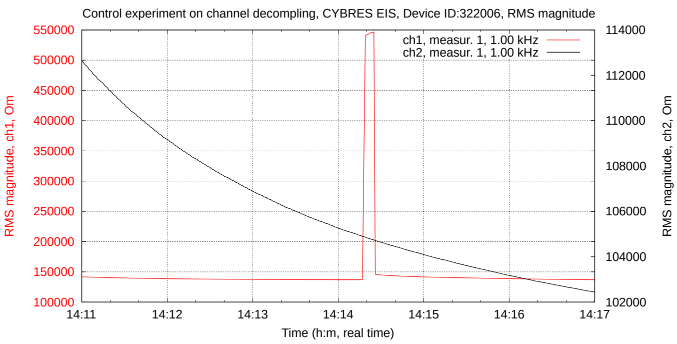


Fig. 31. A control experiment to demonstrate the decoupling of channels, the electrodes in the channel 1 were taken out of the container for a short time, no response in the channel 2 is observed; freshly filled liquids from different sources were used, the noise is set to a minimal level by selecting the excitation voltage in the range 0.1-1V.

manner of coupled oscillators, due to the effects of 'macro-entangled' objects. We also note the occurrence of spikes and 'jumps' in the 'main channel' during the self-excitation of the 'linked channel'.

Experiments shown in Fig. 30 have been repeated several times, one run for fluids freshly filled from different sources is shown in Fig. 32(a), for 'processed' fluids filled from the same source – in Fig. 32(b). We observe here a similar behavior to the previously shown dynamics – a correlation between channels in experimental attempt, whereas the control experiment does not demonstrate any correlation in the same conditions.

The experiments shown in this section have an explorative character. First, the relationship between optical and electrochemical effects is still not fully investigated in physical chemistry. It is possible that the 'nonclassical' character of 'self-excitation' has some (quantum) physical nature. We exclude the parasitic coupling (measuring artifacts) between channels, see the control measurement in Figs. 31 and 32(a), moreover the 'macro-entangled' effect does not always work. It arises, firstly, when the excitation voltage is set to a minimal scale of 0.01V-0.1V, where the signal processing operates at the noise level. This explains the large noise in Figs. 30(b) and 32. Secondly, a weak emission of various nature is almost always present in such experiments. For more strong results, measurements should be performed between fully independent EIS devices and more attempts should be undertaken for accumulation of statistical significance. However, since this work represents a report on experiment, we demonstrate the obtained data and provide such explanations that are available at the moment. It is assumed, as a working hypothesis, that the well-known synchronization effect of coupled oscillators with weak (nonlocal) coupling plays here a key role [43].

## IV. Conclusion

Based on experimental results, we can conclude with sufficient confidence – taking into account difficulties in detecting weak emissions – that the circular CPV emitter with one circular dipole demonstrates effects that are similar to the previously investigated effects of the optical LED emitter [42], [26]. There are observed effects of delayed EIS dynamics, mismatch with temperature curves, the appearance of 'paradoxical phases', accumulation of emission after the generator is turned off. Comparing the axial and radial directions, we note more intense reaction of the EIS sensors in the axial direction at the top of the cone. This is unusual, since both containers are at the distance of 10 cm from each other and should show a similar dynamics, when do not take into account the generated weak emission. Express analysis of the irradiated sample gives results similar to the V.A.Sokolova's group, which were obtained for the Deev's and Akimov's generators. Considering results of liquids exposure, described in Sec. III-D, we note primarily the experimental confirmation of electrochemical differences between exposed and unexposed liquids. Also, a stimulating biological effect on microorganisms is registered in the position at the 'top of the cone'. All specific questions related to PTT effect will be discussed in a separate paper.

The structure of the CPV emitter and the EHM-C module follows the concept of the 'small Akimov's generator' and implies the same applications – a compact, mobile source of generated weak emission that allows scaling

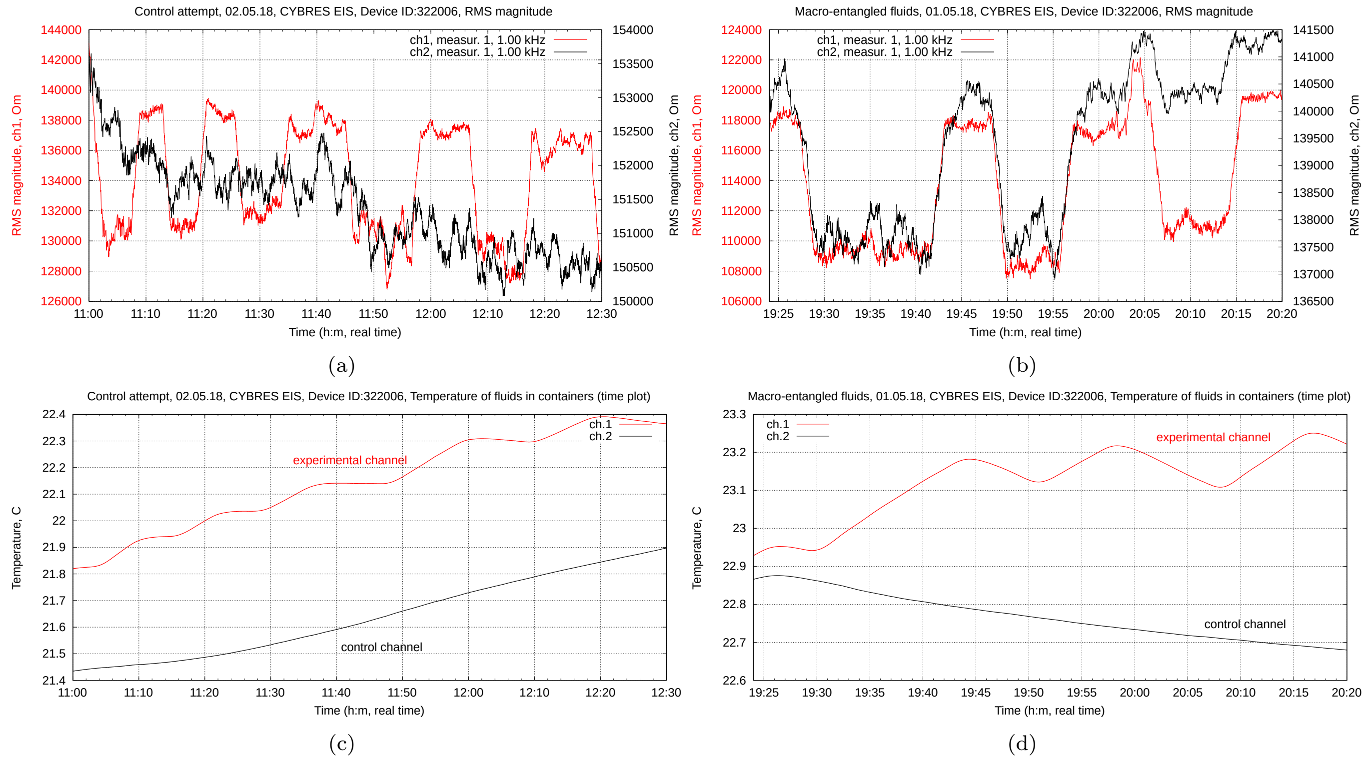


Fig. 32. Replication of the experiment from Fig. 30. **(a)** Control attempts, all parameters are identical to experiment shown in Fig. 32(b), but fluids are filled from different sources, no correlation between channels is observed; **(b)** Experimental attempt, all parameters are identical to the experiment from Fig. 32(a), but fluids are filled from the same source and 'processed' by weak emissions, correlations between channels 1 and 2 are observed (about 10 difference in amplitude between channels); **(c,d)** Temperature dynamics of both channels in control and experimental attempts.

up the irradiation effect. After numerous experiments, we decided to leave the external elements of the generator without grounding - on the one hand this increases its efficiency, but on the other hand it is necessary to keep in mind the arising electrostatic charge. Since the concept of unconventional technologies has changed over the past 20 years, new features have been added to the device: modularity, a set of replaceable emitters and concentrators, combining with the shape effect and the passive 'Contur' system, the possibility of using different physical and electronic modulators. The modern market of unconventional technologies suggests the ineffectiveness of 'securing secrets' and 'strict patenting' strategy, which was followed by the team of A.E.Akimov. We choose more open approach for devices and publications, when the modular generation technology, different encountered effects and detecting/sensing devices are provided to users.

It is necessary to note the feedback methods shown in Sec. III-F. The combination of the DA module, measuring system and actuators (CPV emitter, lasers, electrostatic and LED generators) allow imposing a forced behavior on local and nonlocal objects. This enables a new class of techniques for working with distant objects, such as the 'self-excitation' mode, or synchronization of nonlinear oscillators with weak nonlocal coupling. Obviously, this topic needs further development and a careful treatment of ethical issues.

We point to safety methods when using these technologies, in particular a strong recommendation to limit the intensity of generated weak emissions to requirements of the intended tasks. It is necessary to allocate a separate room for these works and always allow 'draining' emissions through large grounded metal screens and/or a source of flowing water. Since the emissions has the capability to be 'accumulated' on objects, it needs to provide enough time to dissipate the 'accumulated charge'. When using nonlocal effects, it must be noted that a nonlocal interaction is always multi-directional, it combines and provides impacts from all involved sides. Experiments show that it can 'entangle' all participants that use the same modulator or device in a certain time range. In conclusion, we point once again to the ethical principles of working with this technology.

## References

[1] A.E.Akimov, B.I.Petrovsky, and V.J.Tarasenko. *Structure and construction of torsion generators, pre-pring N52 (rus).* M., MNTC VENT, 1995.

[2] O.B.Bron. *Electromagnetic fields as a kind of matter (rus).* M., State Energy Publishing House, 1962.

[3] S.Kernbach, V.T.Shkatov, and V. Zamsha. Report on experiment with super-long range signal transmission by using a digital representation of planet Mars (rus). *International Journal of Unconventional Science*, 2(1):61–75, 2013.

[4] S.Kernbach, A.Kernbach, A.Rusanov, and I.Volkov. Analysis of the ochatrin's detector and the smal akimov's generator. *IJUS*, 9(3):70–89, 2015.

[5] S. Kernbach. Unconventional research in USSR and Russia: short overview. *arXiv 1312.1148*, 2013.

[6] V.I.Lunev. *Experimental research in the field of spin-torsion interactions (rus)*. Tomsk, 1995.

[7] V.N. Anosov and E.M. Truchan. New approach to impact of weak magnetic fields on living objects (rus). *Doklady Akedemii Nauk: biochemistry, biophysics and molecular biology*, (392):1–5, 2003.

[8] E.M Trukhan. Impact of weak electro-magnetic fields on biological activity of water phase (rus). *Computer Research and Modeling*, 1(1):101108, 2009.

[9] Ivan Rampl, Vladimír Boudný, Milan Cíž, Antonín Lojek, and Pavel Hyršl. Pulse vector magnetic potential and its influence on live cells. In *Proceedings of the 2009 International Conference on eHealth, Telemedicine, and Social Medicine*, ETELEMED '09, pages 99–107, Washington, DC, USA, 2009. IEEE Computer Society.

[10] Y. Aharonov and D. Bohm. Significance of Electromagnetic Potentials in the Quantum Theory. *Physical Review Online Archive (Prola)*, 115(3):485–491, 1959.

[11] Vlatko Vedral. Quantifying entanglement in macroscopic systems. *Nature*, 453(7198):1004–1007, 2008.

[12] J. Sperling and I. A. Walmsley. Entanglement in macroscopic systems. *Phys. Rev. A*, 95:062116, Jun 2017.

[13] Olga Bolshakova. *The 'Maslobrod Effect' (rus)*. Russian Word, N13 (641) 6.04.2018, 2018.

[14] Remy Chauvin. A PK experiment with mice. *Journal of the Society for Psychical Research*, (53(804)):348–351, 1986.

[15] Rene Peoc'h. Psychokinetic action of young chicks on the patch of an illumunetaed souirce. *Journal of Scientific Exploration*, (9(2)):223–229, 1995.

[16] M. Odier. Can plants influence chance? *Bulletin de la Fondation Marcel et Monique Odier de Psycho-Physique*, (4):13–17, 1997.

[17] H. Schmidt. PK experiments with animals as subjects. *Journal of Parapsychology*, (34(4)):255–261, 1970.

[18] J. Hagel and M. Tschapke. Zum experimentellen nachweis akausaler korrelationseffekte in unbelebten systemen. *Zeitschrift für Anomalistik*, (2):6–31, 2002.

[19] A.Y.Smirnov. Long-range nonlocal interactions in 'teleportation' of information. *Proc. of II int. conf. 'Torsion fields and information interactions'*, pages 119–149, 2010.

[20] CYBRES. *EIS Differential Impedance Spectrometer for electrochemical and electrophysiological analysis of fluids and organic tissues. User Manual.* Cybertronica Research, 2018.

[21] OPPGT Document No. 1220. *Evaluation of Non-Chemical Treatment Technologies for Cooling Towers at Select California Facilities.* California Department of Toxic Substances Control Office of Pollution Prevention and Green Technology, 2009.

[22] F. Alimi, M.M. Tlili, M. Ben Amor, G. Maurin, and C. Gabrielli. Effect of magnetic water treatment on calcium carbonate precipitation: Influence of the pipe material. *Chemical Engineering and Processing: Process Intensification*, 48(8):1327 – 1332, 2009.

[23] K.K Jyoti and A.B Pandit. Water disinfection by acoustic and hydrodynamic cavitation. *Biochemical Engineering Journal*, 7(3):201 – 212, 2001.

[24] A.V.Kluev, S.A.Kurapov, V.F.Panov, V.V.Strelkov, N.A.Kokarev, and A.E.Boajrishnikov. Structure and mechanical properties of metals after processing in a nonstationary electromagnetic field (rus). *Metallurgy, thermal processing of metals*, (7 (649)):3–9, 2009.

[25] Serge Kernbach, Vitaliy Zamsha, and Yuri Kravchenko. Experimental approach towards long-range interactions from 1.6 to 13798 km distances in bio-hybrid systems. *NeuroQuantology*, 14(3), 2016.

[26] Serge Kernbach. Replication attempt: Measuring water conductivity with polarized electrodes. *Journal of Scientific Exploration*, 27(1):69–105, 2013.

[27] S. Kernbach, I.Kuksin, O.Kernbach, and A.Kernbach. The vernadsky scale – on metrology of EIS in time-frequency domain. *IJUS*, 143–150(5):62–87, 2017.

[28] S. Kernbach, I. Kuksin, and O. Kernbach. Analysis of ultraweak interactions by electrochemical impedance spectroscopy (rus). *IJUS*, 11(4):6–22, 2016.

[29] S. Kernbach, I. Kuksin, and O. Kernbach. On accurate differential measurements with electrochemical impedance spectroscopy. *WATER*, 8:136–155, 2017.

[30] F.J. Millero. *The Physical Chemistry of Natural Waters*. Wiley-Interscience, New York, 2001.

[31] John A. Sorensen and Gary E. Glass. Ion and temperature dependence of electrical conductance for natural waters. *Analytical Chemistry*, 59(13):1594–1597, 1987.

[32] Masaki Hayashi. Temperature-electrical conductivity relation of water for environmental monitoring and geophysical data inversion. *Environmental Monitoring and Assessment*, 96(1):119–128, Aug 2004.

[33] S.Kernbach. On symbols and mems. part 2 (rus). *submitted to IJUS, 19(6)*, 2018.

[34] S. Kernbach. *Supernatural. Scientifically proven facts (rus)*. Algorithm. Moscow, 2015.

[35] T. Hieronymus. Growing plants without sunlight, 1931.

[36] V.A. Sokolova. *First experimental confirmation of torsion fields and their usage in agriculture (rus)*. Moscow, 2002.

[37] Yury Nepomnyashchiy, Olga Kernbach, Igor Kuksin, Andreas Kernbach, Timo Dochov, Andrew Bobrov, and Serge Kernbach. The biosensor based on measurements of zymase activity of yeast *Saccharomyces Cerevisiae. (submitted) Biosensors.*

[38] S. Kernbach and O. Kernbach. Detection of ultraweak interactions by precision dph approach (rus). *IJUS*, 9(3):17–41, 2015.

[39] Serge Kernbach and Olga Kernbach. Impact of structural elements on high frequency non-contact conductometry. *IJUS*, 12-13(4):47–68, 2016.

[40] Laboratory of Advanced Sensors. *Preliminary report: Evaluation Of water/DVD samples from the live event on 31.10.15 in Esslingen by Braco (The Project No. 311015-3492-De)*. Cybertronica Research, 2015.

[41] V.T. Shkatov. *On interactions between the device for measuring weak emission and its developper (rus)*. Vesnik NO EIT MAEI, N7, pp.21-31, Barnaul, 'Statistika', 2010.

[42] S. Kernbach. Exploration of high-penetrating capability of LED and laser emission. Parts 1 and 2 (rus). *Nano- and microsystem's technics*, 6,7:38–46,28–38, 2013.

[43] P. Levi, M. Schanz, S. Kornienko, and O. Kornienko. Application of order parameter equation for the analysis and the control of nonlinear time discrete dynamical systems. *Int. J. Bifurcation and Chaos*, 9(8):1619–1634, 1999.

## Appendix

# EHM-C control module

## for generators of alternating electric and magnetic fields, DC motors, LED emitters with variable intensity, precise dual-output thermostats


EHM-C module is a control circuit for generators of alternating electric and magnetic fields. Two DC motors can be also connected as an inductive load. Additionally, the scheme is utilized for controlling LED emitters with variable brightness, as well as in the high-voltage/ultrashort-pulses mode. With external temperature sensors LM35/AD592, the module has a functionality of dual-output (heater/cooler) digital thermostat with PID controller. The EHM-C module consists of four parts: the high voltage generator (5-1200V), the controller of inductive load (5-40V, 2A, reversible); the controller of a high current load (5-30V, up to 100A (500A) impulse current) and a microcontroller system for modulating all outputs with up to 5MHz of the carrier frequency and the secondary low-frequency 0.7Hz - 1kHz modulation. The module is powered from USB when the consumed average current is less than 0.5A (0.9A), a higher load current requires an external power supply. The module has an internal 5V to 40V (3A) voltage converter. Heat dissipation capacity is about 2W, an external heat sink is required to dissipate more heat. Management - enabling and disabling outputs, setting voltages and frequencies, programming timers and PID controller to operate in autonomous mode – is possible via USB by using a client program or by ASCII commands. The advantage of this module is the capability to control combined opto- magneto- electric devices, to use standard USB batteries for mobile applications, to operate autonomously without external control. Due to a small size, the EHM-C module can be easily integrated into other devices and systems.

### Features

- input voltage: 5-30V
- integrated voltage converter 5V to 40V, 3A
- output voltage E (for electric field emitters): 5-1200V (B/I/H versions only)
- output voltage H (for magnetic field emitters or DC motors): 5-40V, 2A, with the possibility of reverse current
- output voltage L (for high power LED emitters, inductive load, various DC devices): 5-40V, up to 100A (500A) impulse current
- Pulse Width Modulation of output voltages with 0-5MHz of currier frequency
- secondary low-frequency modulation 0.7Hz – 1kHz (rectangular pulses) of all outputs
- programmable timers: 100ns-72 hours
- resolution of relative temperature measurement: 0.01°C
- PID controller with adjustable coefficients
- I2C, SPI, UART, USB interfaces
- size: 100x36x8мм

### Application

- combined opto- magneto- electric systems and generators
- generators of alternating electric and magnetic fields
- systems for exploring electric and magnetic Aharonov-Bohm effect, the Graham-Lahoza experiment, and similar combined electric and magnetic systems
- experimental generators of magnetic vector potential
- phase-synchronized control of DC motors
- control of LED emitters with variable brightness
- high-voltage/ultrashort-pulses mode for LED emitters
- increasing voltage to 18V/40V or up to 1200V from USB
- switching (on-off, PWM) of different DC devices at up to 40V and a high impulse current
- precise universal thermostats with dual heater/cooler outputs
- remote temperature data loggers